PROCEEDINGS OF SCIENCE

The ρ radiative decay width from lattice QCD

Marcus Petschlies[*†]
Helmholtz-Institut für Strahlen- und Kernphysik, Bonn University
E-mail: marcus.petschlies@hiskp.uni-bonn.de

Constantia Alexandrou
Computation-based Science and Technology Research Center, Cyprus Institute,Department of Physics, University of Cyprus
E-mail: c.alexandrou@cyi.ac.cy

Luka Leskovec
Jefferson Lab
E-mail: leskovec@jlab.org

Stefan Meinel, Gumaro Rendon
Department of Physics, University of Arizona
E-mail: smeinel@email.arizona.edu, jgrs@email.arizona.edu

John W. Negele, Andrew Pochinsky
Center for Theoretical Physics, Laboratory for Nuclear Science and Department of Physics, Massachusetts Institute of Technology
E-mail: negele@mit.edu, avp@mit.edu

Srijit Paul
Computation-based Science and Technology Research Center, Cyprus Institute
E-mail: s.paul@cyi.ac.cy

Sergey Syritsyn
Department of Physics and Astronomy, Stony Brook University
E-mail: syritsyn@gmail.com

Pion photoproduction constitutes a prototype process, which allows for the study of the electroweak decay of a QCD-unstable state, the ρ resonance. It is also the most straightforward process to investigate such (resonant) transition matrix elements in lattice QCD. We performed a lattice calculation of the process $\pi\pi \to \rho \to \pi\gamma$, at presently the lightest pion mass of 317 MeV and in a large box of size $(3.6\,\mathrm{fm})^3$. In addition to outlining the method for our calculation, we give account of our analysis of systematic uncertainties, with focus on parametrization dependence of the $P-$wave phase shift and the analytic continuation of our lattice data to the ρ resonance pole to extract the coupling $|G_{\rho\pi\gamma}| = 0.0802\,(38)$.

The 9th International workshop on Chiral Dynamics
17-21 September 2018
Durham, NC, USA

*Speaker.
†for the LHPC-Cyprus-Bonn group

PoS(CD2018)080

1. Introduction

The calculation of electro-weak matrix elements of QCD-unstable hadronic states has been of long-standing interest to lattice QCD. Calculations in lattice QCD are performed in Euclidean, discretized space-time and in a finite volume box of size $L^3 \times T$. Within this setup, S-matrix elements are not directly accessible from lattice n-point correlation functions. Indeed, Maiani and Testa's no-go theorem [1] stated early on, that inescapable final state interactions of multi-hadron states in finite volume prevent a straight-forward interpretation of matrix elements from the lattice in terms of continuum and infinite-volume amplitudes.
This issue of proper normalization of lattice correlation functions during conversion to infinite volume has been addressed for the case of the K to $\pi\pi$ transition in the pioneering work by Lellouch and Lüscher [2], based on the Lüscher quantization condition [3] for 2-hadron states in finite volume and the mapping of the finite-volume lattice spectrum to the elastic scattering amplitude. More recently, Briceño, Hansen and Walker-Loud (BHWL) generalized the method for these $1 \to 2$ transitions to arbitrary current insertions between the single- and two-hadron initial and final state, with arbitrary momentum transfer, as well as fields with arbitrary spin [4, 5]. A prototype calculation for the $\pi\gamma \to \pi\pi$ transition was presented in [6, 7].
In this contribution we present our calculation of the pion-photo-transition amplitude at so far lightest pion mass of 317 MeV, We focus in particular on the ρ-resonance region to extract $\rho - \pi - \gamma$ coupling and the photoproduction cross-section. The further implementation of the BHWL formalism opens the exciting prospect to study more complicated electro-weak matrix elements for resonant transitions, such as for nucleon-pion and nucleon-kaon.

2. Resonant pion-photoproducion process

The pion-photo production amplitude across the ρ-resonance region is the most straightforward example to start with and we give a pictorial representation in Fig. 1. In continuum and

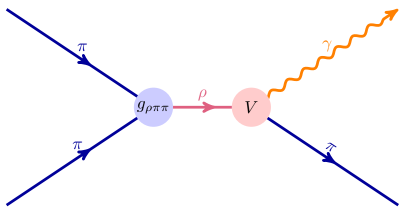

Figure 1: Diagram representation for resonant photoproduction with $g_{\rho\pi\pi}$ coupling (left vertex) and photo-transition amplitude.

infinite volume QCD, the decomposition of the matrix element is governed by Lorentz symmetry and given by

$$\langle \pi\pi \,|\, J^\mu(0) \,|\, \pi \rangle = \frac{2\mathrm{i}\, \mathcal{V}_{\pi\gamma\to\pi\pi}(q^2, s)}{m_\pi}\, \varepsilon^{\nu\mu\alpha\beta}\, \varepsilon_\nu(P, m)\, (p_\pi)_\alpha P_\beta \,. \tag{2.1}$$

P denotes the total 4-momentum of the final 2-pion state, p_π that of the initial single-pion state, $\sqrt{s}$ the invariant mass and ε the polarization 4-vector for the $\pi\pi$ P-wave state $\langle l = 1,\, m|$.

Splitting off the kinematic factors introduces the photo-transition amplitude $\mathscr{V}_{\pi\gamma\to\pi\pi}$ depending on invariant mass and photon momentum transfer $q^2 = (P - p_\pi)^2$. Given the normalization with inverse pion mass chosen in (2.1) and the normalization of single- and 2-pion states [1] , the amplitude $\mathscr{V}_{\pi\gamma\to\pi\pi}$ has units of MeV^{-1}.

The residue of the elastic $\pi\pi$ isospin-1 scattering amplitude $\mathscr{T}_{\pi\pi\to\pi\pi}$ at the ρ resonance pole $s_P \approx m_R^2 + i m_R \Gamma_R$ defines the coupling $G_{\rho\pi\pi}$: in the vicinity of s_P the scattering amplitude is given by

$$\mathscr{T}_{\pi\pi\to\pi\pi} = \frac{16\pi\sqrt{s}}{k}\,\frac{1}{\cot(\delta(s)) - i} \underset{s\to s_P}{\sim} \frac{G_{\rho\pi\pi}^2}{s_P - s} \tag{2.2}$$

with $\pi\pi$ center-of-mass momentum k and elastic scattering phase shift $\delta(s)$.

The photo-production amplitude has a pole at the ρ resonance as well. Moreover, its complex phase is determined by the final state interaction of the 2 pions, i.e. by the $\pi\pi$ scattering phase shift, according to Watsons's Theorem. Thus, factoring out the pole and observing the phase $\mathscr{V}_{\pi\gamma\to\pi\pi}$ can be written in terms of the form factor $F(q^2, s)$ in Eq. (2.3),

$$\mathscr{V}_{\pi\gamma\to\pi\pi}(q^2, s) = \sqrt{\frac{16\pi}{k\Gamma(s)}}\,\frac{F(q^2, s)}{\cot(\delta(s)) - i} \underset{s\to s_P}{\sim} \frac{G_{\rho\pi\pi}\,G_{\rho\pi\gamma}}{s_P - s}\,. \tag{2.3}$$

3. Biceño-Hansen-Walker-Loud formalism

The calculation of the transition amplitude for the process $\pi\gamma^* \to \rho$ requires a matrix element with the ρ as final state. By virtue of decay to two pions[2] the ρ is QCD-unstable and the normalization of the matrix elements obtained from lattice QCD in finite volume requires the proper residual of the fully dressed 2-pion propagator arising from the infinite sequence of elastic rescattering, which is unavoidable in the finite lattice volume. The corresponding finite to infinite volume conversion has been introduced for the $K \to \pi\pi$ process in [2], has recently been generalized as the Briceño-Hansen-Walker-Loud (BHWL) formalism [4, 5] and accommodates the case considered here, which was first applied in [6, 7]. The BHWL work-flow we follow is captured in the chart 2: the finite-volume spectrum in the ρ channel is determined from the lattice calculation and converted into the scattering amplitude at the discrete finite-volume energy levels via the Lüscher quantization condition. Together with the finite-volume $1 \to 2$ matrix elements input, the BHWL formalism gives the corresponding infinite-volume transition amplitude evaluated at the lattice energy levels, which are subsequently analytically continued to the ρ resonance pole. The pole location we obtain from describing our scattering amplitude data with the Breit-Wigner form and variations thereof.

[1] The normalization is chosen as follows:

$$\begin{aligned}\langle \pi(p)\,|\,\pi(q)\rangle &= 2E(\vec{p})\,(2\pi)^3\delta^{(3)}(\vec{p}-\vec{q})\\ \langle \pi\pi, P, \vec{k}_{\mathrm{CM}}\,|\,\pi\pi, P', \vec{k}'_{\mathrm{CM}}\rangle &= 2E_1\,2E_2\,(2\pi)^3\delta^{(3)}(\vec{k}-\vec{k}')\,(2\pi)^3\delta^{(3)}(\vec{P}-\vec{k}-\vec{P}'+\vec{k}')\end{aligned}$$

[2] Below the $K\bar{K}$ and 4π threshold.

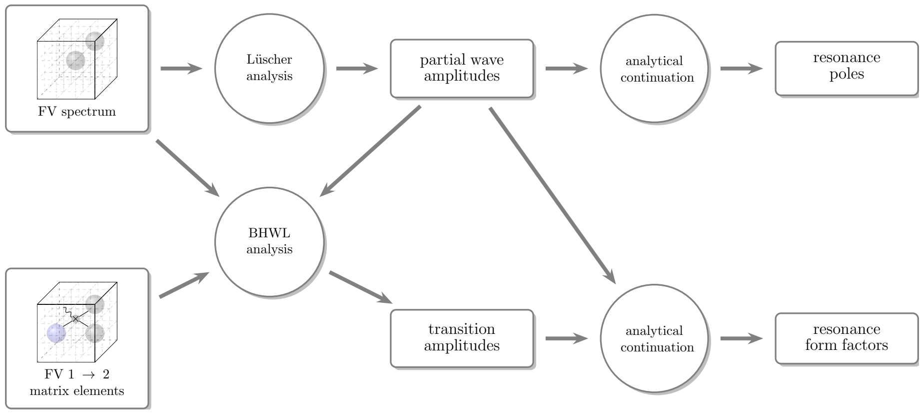

Figure 2: Workflow chart for the Briceño-Hansen-Walker-Loud formalism [4, 5]

4. Elastic $\pi\pi$ isospin-1 $p-$wave phase-shift

To extract the lattice spectrum in the ρ-channel $I\,(J^P) = 1\,(1^-)$ we solve the generalized eigenvalue problem (GEVP) [8, 9] for correlation matrices built from a variational basis of single hadron (quark-bilinear, or ρ-type) and two-hadron ($\pi\pi$-type) interpolating fields. The matrices of 2-point correlation functions are considered per $\pi\pi$ center-of-mass momentum and projected to irreducible representations (irreps) of the lattice, finite-volume rotational symmetry group O_h and subgroups thereof.

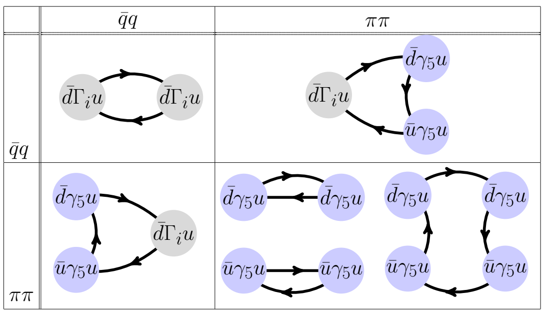

Figure 3: Schematic representation of diagrams arising from Wick contractions

$\vec{P}\ [\frac{2\pi}{L}]$	$LG(\vec{P})$	Irrep Λ	ℓ
$(0,0,0)$	O_h	T_1^-	$1^-,3^-,\ldots$
$(0,0,1)$	C_{4v}	A_2^-	$1^-,3^-,\ldots$
$(0,0,1)$	C_{4v}	E^-	$1^-,3^-,\ldots$
$(0,1,1)$	C_{2v}	B_1^-	$1^-,3^-,\ldots$
$(0,1,1)$	C_{2v}	B_2^-	$1^-,3^-,\ldots$
$(0,1,1)$	C_{2v}	B_3^-	$1^-,3^-,\ldots$
$(1,1,1)$	C_{3v}	A_2^-	$1^-,3^-,\ldots$
$(1,1,1)$	C_{3v}	E^-	$1^-,3^-,\ldots$

Table 1: Lattice rotational symmetric groups, irreps and angular momentum content considered in this work

The pertinent prototypes of Wick contractions are shown in the left-hand side figure above. The right-hand side table lists the total $\pi\pi$ momentum vectors $\vec{P}$, the corresponding residual rotational symmetry or little groups $LG(\vec{P})$ together with exploited irreps considered in our calculation. The details of construction of Wick diagrams, projection, GEVP analysis and conversion to scattering amplitude for our study are given in [10]. The parameters for our lattice calculation are collected in table 2; the gauge field ensemble (“C13”) was provided by Kostas Orginos et al. and generated using XSEDE resources.

We summarize our results (in lattice units) for the $\pi\pi$ elastic phase shift and model interpola-

Label	a / fm	L / fm	m_π / MeV	m_K / MeV	$m_\pi L$
`C13`	0.11403 (77)	3.649 (25)	≈ 317	≈ 530	5.865 (32)

Table 2: Parameters for ensemble `C13` used during our study.

tion in the left-hand side figure and the table below.

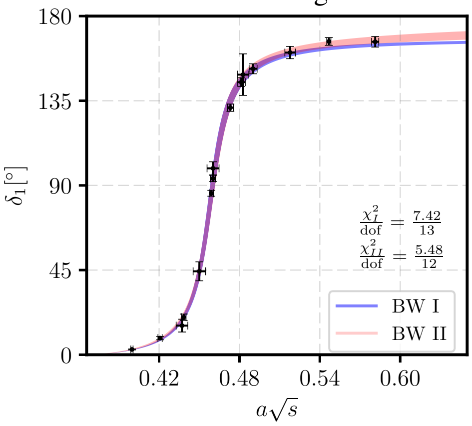

	BWI	BWII
$\frac{\chi^2}{\mathrm{dof}}$	0.571	0.457
am_ρ	0.4599 (19) (13)	0.4600 (18) (13)
$g_{\rho\pi\pi}$	5.76 (16) (12)	5.79 (16) (12)
$(ar_0)^2$	$---$	8.6 (8.0) (1.2)

The 15 kinematic points in invariant $\pi\pi$ mass $\sqrt{s}$ are fitted to Breit-Wigner models denoted "BWI" and "BWII"

$$\text{BWI} \;\; \Gamma_I(s) = \frac{g^2_{\rho\pi\pi}}{6\pi}\frac{k^3}{s} \tag{4.1}$$

$$\text{BWII} \;\; \Gamma_{II}(s) = \frac{g^2_{\rho\pi\pi}}{6\pi}\frac{k^3}{s}\,\frac{1+(k_R r_0)^2}{1+(kr_0)^2} \tag{4.2}$$

BWII amends the standard BWI form by a Blatt-Weisskopf barrier factor with radius r_0. The results for the fit parameters are given in the table above. With BWII we do not detect significant deviations from the simple BWI form. Yet in the BHWL analysis to follow, we keep both parametrizations to check for systematic uncertainties originating from the choice of interpolation model.

5. Photoproduction amplitude

The finite-volume transition matrix element $\langle \pi, \vec{p}_\pi \,|\, J_\mu(0,\vec{Q}) \,|\, n, \vec{P}, \Lambda, r\rangle$ is determined for the nth energy level with a given total momentum $\vec{P}$ of the $\pi\pi$ system, which is projected to row r within irrep Λ. We obtained it from 3-point functions using the variationally optimized interpolators, that result from the GEVP analysis, with the insertion of the multiplicatively renormalized ([11]) electromagnetic current $J_\mu = Z_V\,\left(\frac{2}{3}\,\bar{u}\,\gamma_\mu\,u - \frac{1}{3}\,\bar{d}\,\gamma_\mu\,d\right)$ between initial 2-pion and final single-pion state interpolator as given in Eq. (5.1)

$$\Omega^{\vec{p},\vec{P},\Lambda,r}_{3,\mu,n}(t_\pi, t_J, t_{\pi\pi}) \;=\; \langle \mathcal{O}^{\vec{p}_\pi}_\pi(t_\pi)\;\; J_\mu(t_J,\vec{q})\;\; \mathcal{O}^{n,\vec{P},\Lambda,r}(t_{\pi\pi},\vec{P})^\dagger \rangle\,. \tag{5.1}$$

For large time separations between final / initial state excitation and current insertion $t_{\pi\pi} - t_J \,/\, t_\pi - t_J$ the ensuing ratio (5.2) of 3-point and 2-point functions is proportional to the desired finite-volume

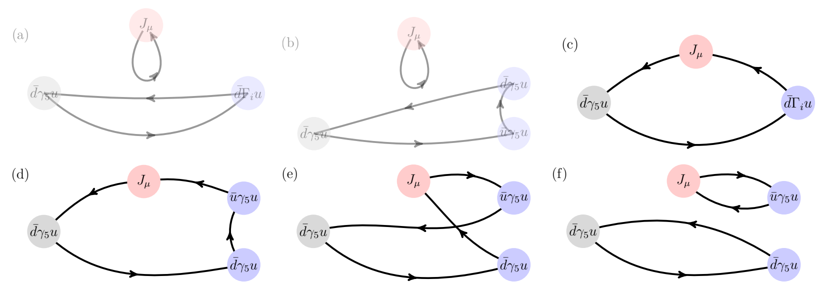

Figure 4: Diagrams for the 3-point functions from quark-bilinear and 2-hadron interpolators with vector current insertion. Partially transparent, quark-disconnected diagrams are neglected.

matrix element up to excited state contamination.

$$\begin{aligned} R_{\mu,n}^{\vec{p},\vec{P},\Lambda,r}(t_\pi,t_J,t_{\pi\pi}) &= \frac{\Omega_{3,\mu,n}^{\vec{p},\vec{P},\Lambda,r}(t_\pi,t_J,t_{\pi\pi})\,\Omega_{3,\mu,n}^{\vec{p},\vec{P},\Lambda,r}(t_{\pi\pi},t_{\pi\pi}+t_\pi-t_J,t_\pi)}{C_\pi^{2pt}(t_\pi-t_{\pi\pi})\,C_{n,\vec{P},\Lambda,r}^{2pt}(t_\pi-t_{\pi\pi})} \\ &\overset{t_{\pi\pi/\pi}-t_J\ \text{large}}{\propto} |\langle \pi,\vec{p}_\pi \mid J_\mu(0,\vec{Q}=\vec{p}_\pi-\vec{P}) \mid n,\vec{P},\Lambda,r\rangle|_{FV}^2 \end{aligned} \tag{5.2}$$

We depict the prototype Wick contractions used to build the 3-point functions in Fig. 4. The partially transparent top left and center diagrams are quark-disconnected with the vector current loop. The contribution of those diagrams are statistically insignificant for the signal at our present level of accuracy and neglected in our calculation. An exemplary subset of ratios for total momenta $|\vec{P}| = \sqrt{3}\,2\pi/L$ and $|\vec{P}| = 2\pi/L$ for several irreps together with the fits to a constant is shown in the 3 left-hand columns of Fig. 5: the three columns correspond to source-sink time separation $t_\pi - t_{\pi\pi} = 8a,\ 10a,\ 12a$. The right-most column shows the stability of the constant fit under variation of data selected into the fit from the set of source-sink separations and number of data points around the center $t_J = (t_\pi - t_{\pi\pi})/2$.

Following the BHWL formalism in Fig. 2, we convert the finite-volume matrix element to its infinite-volume counterpart at the same kinematic parameters using the Lellouch-Lüscher factor

$$\frac{|\langle \pi,\vec{p}_\pi|J_\mu(0)|s,q^2;\vec{P},\Lambda,r\rangle_{IV}|^2}{|\langle \pi,\vec{p}|J_\mu(0,\vec{Q})|n,\vec{P},\Lambda,r\rangle_{FV}|^2} = \frac{1}{2E_n^{\vec{P},\Lambda}}\,\frac{16\pi\sqrt{s_n^{\vec{P},\Lambda}}}{k_n^{\vec{P},\Lambda}}\left(\frac{\partial\delta}{\partial E}+\frac{\partial\phi^{\vec{P},\Lambda}}{\partial E}\right)\Bigg|_{E=E_n^{\vec{P},\Lambda}} \tag{5.3}$$

In eq. (5.3) δ denotes the $\pi\pi$ elastic phase shift, $k_n^{\vec{P},\Lambda}$ the $\pi\pi$ center of mass relative momentum and $\phi^{\vec{P},\Lambda}$ is an analytically known function from the Lüscher quantization condition. We show the numerical values for the Lellouch-Lüscher (LL) factor as a function of $\pi\pi$ center of mass energy for our setup in Fig. 6 for all $\pi\pi$ total momenta and irreps used in our calculation. Since the LL factor depends on the interpolation of phase shift data, we show the values for both BWI (blue solid line) and BWII (red dashed line). To appreciate the impact of the scattering phase derivative on the LL factor, in black solid line we give the contribution from $\phi^{\vec{P},\Lambda}$ in eq. (5.3) alone. The left-hand plot in Fig. 7 summarizes our lattice data [12] for the infinite-volume transition amplitude $\mathscr{V}_{\pi\gamma\to\pi\pi}(q^2,s)$ (the complex phase as given by Watson's Theorem is omitted): central values are shown by gray columns, and magenta boxes give the one-standard deviation intervals. To parameterize the data

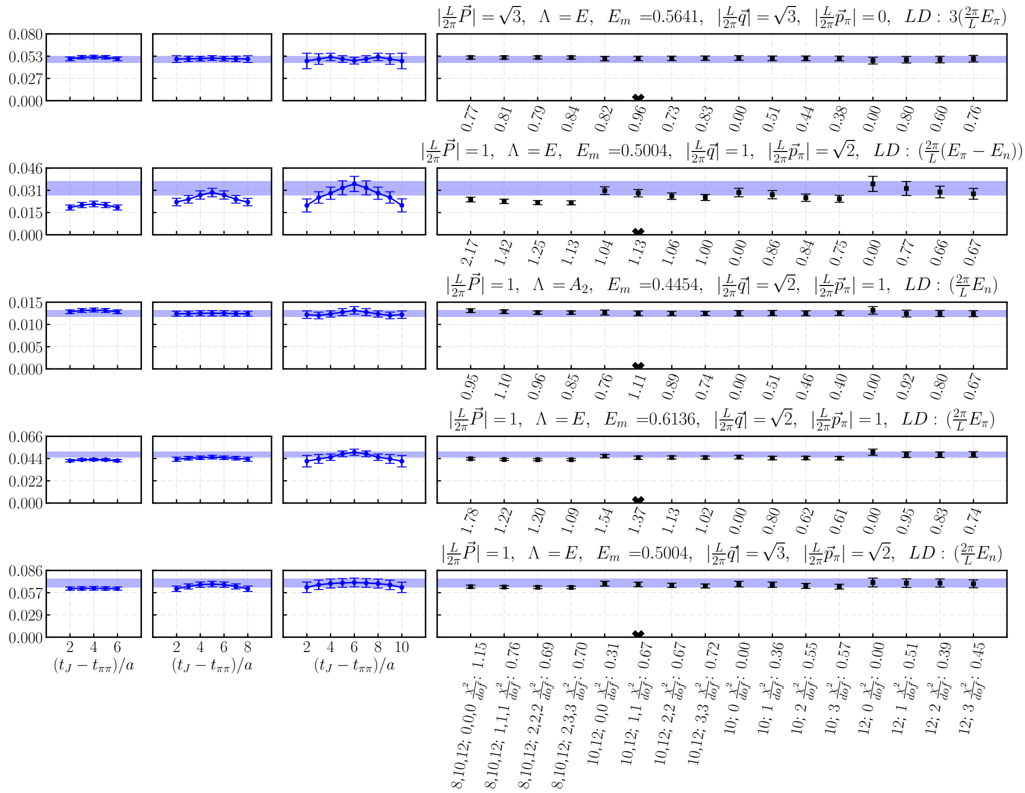

Figure 5: Selection of finite volume matrix element data and fits.

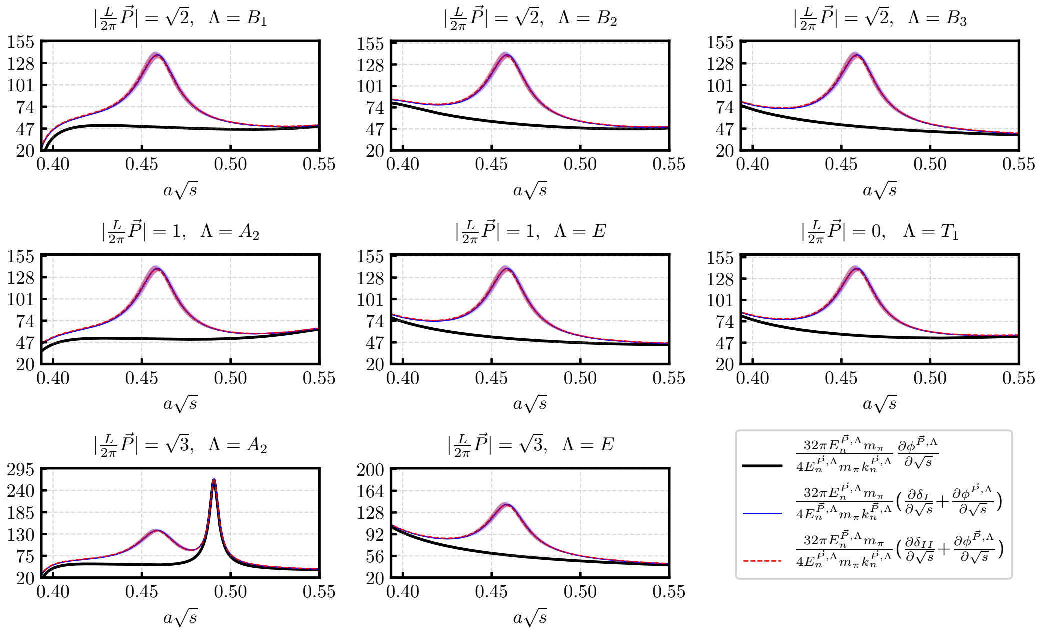

Figure 6: Numerical values for the Lellouch-Lüscher factor

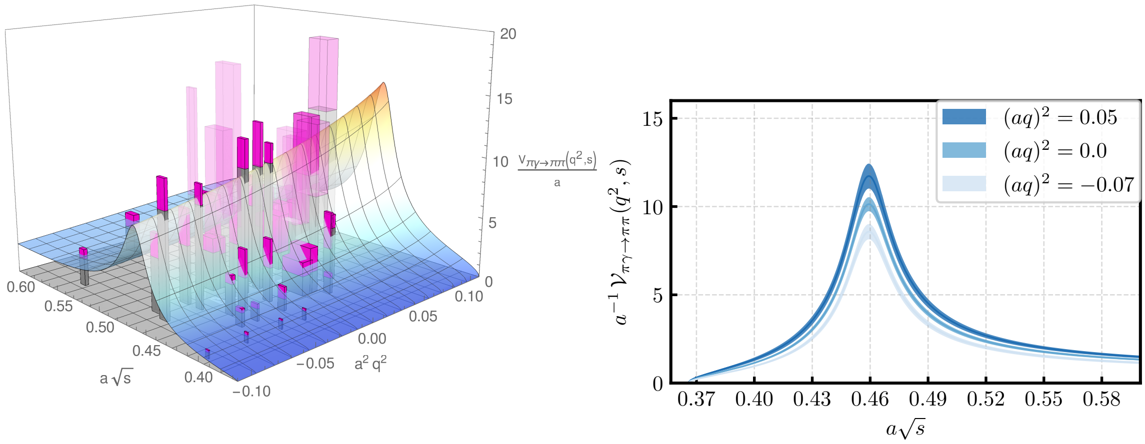

Figure 7: Photo-production amplitude: lattice data (gray columns with magenta one standard deviation interval) and surface of the nominal fit.

we employ a Taylor expansion of the form factor F (cf. eq. (2.3)) in s and q^2 represented by the variables $\mathscr{S} = (s - m_R^2)/m_R^2$ and $z = \frac{\sqrt{t_+ - q^2} - \sqrt{t_+ - t_0}}{\sqrt{t_+ - q^2} + \sqrt{t_+ - t_0}}$:

$$F(q^2, s) = \frac{1}{1 - \frac{q^2}{m_P^2}} \sum_{n=0}^{N} \sum_{m=0}^{M} A_{nm}\, z^n\, \mathscr{S}^m\,, \tag{5.4}$$

where in eq. (5.4) we explicitly factor out the expected pole in q^2 at the resonance pole mass and we use three sequences of cut-off schemes in the number of parameters A_{nm} to probe systematic dependence on the choice of fit model [12]. As an example, the surface in the left-hand plot of Fig. 7 shows our nominal fit result in the s-q^2-plane. Notably, as shown by the sections for constant q^2 on the right-hand plot of Fig. 7, the fall-off of the amplitude for $\sqrt{s}$ larger than the resonance mass is slower than expected for pure resonant behavior.

Finally, in Fig. 8 we show the analytic continuation $F_{\pi\gamma\to\rho}(q^2) = F_{\pi\gamma\to\pi\pi}(q^2, s = s_P)$ in the complex s-plane to the ρ pole. We find the imaginary part (dashed line with green error band) almost consistent with zero. The dark-shaded error bands give the combined statistical and complete systematic uncertainty of $F_{\pi\gamma\to\pi\pi}(q^2, s = s_P)$ up to the choice of parametrization in eq. (5.4). The latter uncertainty is included within the light-shaded error bands.

As a pertinent observable we can determine the $\pi\gamma \to \pi\pi$ photo-production cross section from $\mathscr{V}_{\pi\gamma\to\pi\pi}$,

$$\sigma_{\pi\gamma\to\pi\pi}(s, q^2) = \frac{e^2}{16\pi}\, k\, \frac{4\,|\mathscr{V}_{\pi\gamma\to\pi\pi}(q^2, s)|^2}{m_\pi^2}\,. \tag{5.5}$$

The cross-section for a real photon, eq. (5.5) continued to $q^2 = 0$, is shown in the left-hand plot of Fig. 9. With dark/light-shaded error bands we again distinguish the uncertainty excluding/including the model choice for F.

From the analytically continued form factor $F_{\pi\gamma\to\rho}(q^2)$ at $q^2 = 0$ we obtain the radiative decay

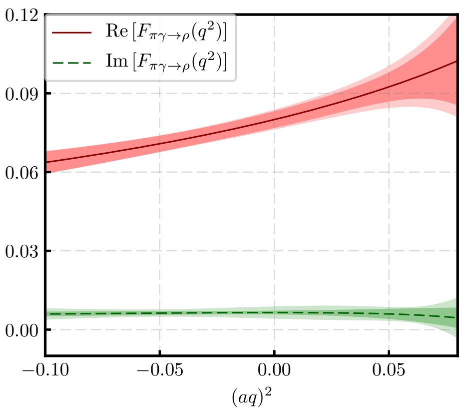

Figure 8: Analytic continuation of the form factor to the ρ pole

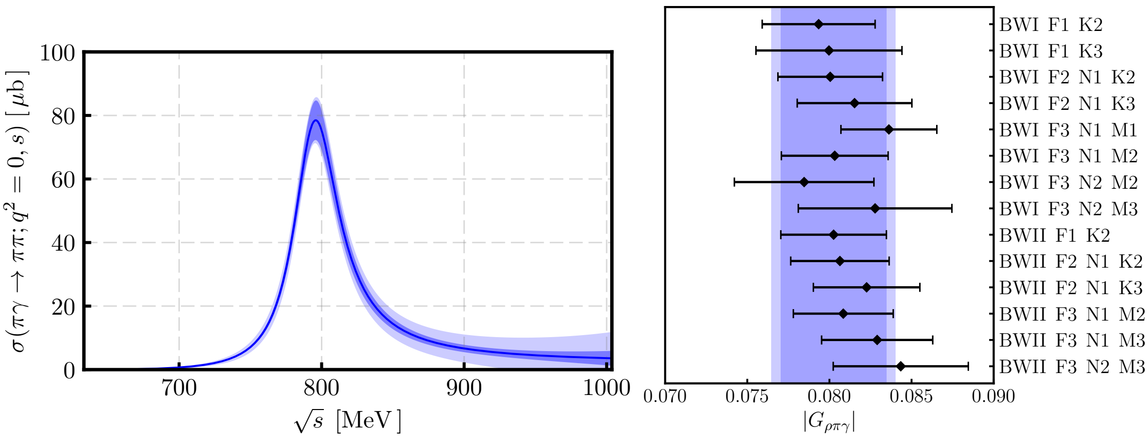

Figure 9: Left: Photo-production cross-section depending on $\pi\pi$ center-of-mass energy; right: Dependence of the numerically extracted ρ-π-γ coupling on the fit model.

width of the ρ as

$$\Gamma(\rho \to \pi\gamma) = \frac{2}{3}\alpha \left(\frac{(m_\rho^2 - m_\pi^2)}{2m_\rho}\right)^3 \frac{|G_{\rho\pi\gamma}|^2}{m_\pi^2} \tag{5.6}$$

parameterized by the coupling $G_{\rho\pi\gamma}$ introduced in eq. (2.2). For the coupling we find

$$|G_{\rho\pi\gamma}| = 0.0802\,(32)\,(20)\,, \tag{5.7}$$

where the first uncertainty is statistical and systematic and the second uncertainty represents the model dependence for $F_{\pi\gamma\to\rho}(0)$, which is shown in detail for all accepted parametrizations of the form factor in the right-hand plot of Fig. 9. Using physical, PDG-values [13] for the particle masses to have realistic kinematics and assuming a negligible pion-mass dependence of the dimensionless coupling $G_{\rho\pi\gamma}$ we thus obtain for the radiative decay width

$$\begin{aligned}
\Gamma(\rho \to \pi\gamma)_{\mathrm{lat}} &= 84.2\,(6.7)\,(4.3)\,\mathrm{keV}\ [\text{physical } m_\pi, m_\rho] \\
\Gamma(\rho \to \pi\gamma)_{\mathrm{exp}} &= 68\,(7)\,\mathrm{keV}\ [13]\,,
\end{aligned}$$

in reasonable agreement with experiment.

6. Outlook

Our continuing work focuses on calculations at smaller pion mass ($m_\pi \sim 170\,\mathrm{MeV}$) to investigate the chiral extrapolation as well as smaller lattice spacing to check for lattice artifacts. Moreover, using our extended analysis framework and our already obtained data, we perform the BHWL analysis for the heavy meson decay processes $B \to (\rho \to \pi\pi)\,\ell\,\bar{\nu}_\ell$ and $B \to (K^* \to K\pi)\,\ell\ell$.

Acknowledgments

MP gratefully acknowledges support by the Sino-German CRC 110.

References

[1] L. Maiani and M. Testa, "Final state interactions from Euclidean correlation functions," *Phys. Lett.*, vol. B245, pp. 585–590, 1990.

[2] L. Lellouch and M. Lüscher, "Weak transition matrix elements from finite volume correlation functions," *Commun.Math.Phys.*, vol. 219, pp. 31–44, 2001.

[3] M. Lüscher, "Two-particle states on a torus and their relation to the scattering matrix," *Nuclear Physics B*, vol. 354, no. 2, pp. 531 – 578, 1991.

[4] R. A. Briceño, M. T. Hansen, and A. Walker-Loud, "Multichannel $1 \to 2$ transition amplitudes in a finite volume," *Phys. Rev.*, vol. D91, no. 3, p. 034501, 2015.

[5] R. A. Briceño and M. T. Hansen, "Multichannel $0 \to 2$ and $1 \to 2$ transition amplitudes for arbitrary spin particles in a finite volume," *Phys. Rev.*, vol. D92, no. 7, p. 074509, 2015.

[6] R. A. Briceño, J. J. Dudek, R. G. Edwards, C. J. Shultz, C. E. Thomas, and D. J. Wilson, "The resonant $\pi^+\gamma \to \pi^+\pi^0$ amplitude from Quantum Chromodynamics," *Phys. Rev. Lett.*, vol. 115, p. 242001, 2015.

[7] R. A. Briceño, J. J. Dudek, R. G. Edwards, C. J. Shultz, C. E. Thomas, and D. J. Wilson, "The $\pi\pi \to \pi\gamma^\star$ amplitude and the resonant $\rho \to \pi\gamma^\star$ transition from lattice QCD," *Phys. Rev.*, vol. D93, no. 11, p. 114508, 2016.

[8] M. Lüscher and U. Wolff, "How to calculate the elastic scattering matrix in two-dimensional quantum field theories by numerical simulation," *Nuclear Physics B*, vol. 339, no. 1, pp. 222 – 252, 1990.

[9] A. collaboration, B. Blossier, M. D. Morte, G. von Hippel, T. Mendes, and R. Sommer, "On the generalized eigenvalue method for energies and matrix elements in lattice field theory," *Journal of High Energy Physics*, vol. 2009, pp. 094–094, apr 2009.

[10] C. Alexandrou, L. Leskovec, S. Meinel, J. Negele, S. Paul, M. Petschlies, A. Pochinsky, G. Rendon, and S. Syritsyn, "P-wave $\pi\pi$ scattering and the ρ resonance from lattice QCD," *Phys. Rev.*, vol. D96, no. 3, p. 034525, 2017.

[11] J. Green, N. Hasan, S. Meinel, M. Engelhardt, S. Krieg, J. Laeuchli, J. Negele, K. Orginos, A. Pochinsky, and S. Syritsyn, "Up, down, and strange nucleon axial form factors from lattice QCD," *Phys. Rev.*, vol. D95, no. 11, p. 114502, 2017.

[12] C. Alexandrou, L. Leskovec, S. Meinel, J. Negele, S. Paul, M. Petschlies, A. Pochinsky, G. Rendon, and S. Syritsyn, "$\pi\gamma \to \pi\pi$ transition and the ρ radiative decay width from lattice qcd," *Phys. Rev. D*, vol. 98, p. 074502, Oct 2018.

[13] C. Patrignani *et al.*, "Review of Particle Physics," *Chin. Phys.*, vol. C40, no. 10, p. 100001, 2016.